

**Near-field mapping of the electromagnetic field in confined photon geometries**

V. Zhuk, D.V. Regelman, and D. Gershoni

*Physics Department and Solid State Institute, Technion-Israel Institute of Technology, Haifa 32000, Israel*

M. Bayer,\* J.P. Reithmaier, and A. Forchel

*Technische Physik, Universität Würzburg, Am Hubland, D-97074 Würzburg, Germany*

P.A. Knipp

*Christopher Newport University, Newport News, Virginia 14728*

T.L. Reinecke

*Naval Research Laboratory, Washington, DC 20375*

(Received 13 March 2002; revised manuscript received 19 June 2002; published 3 September 2002)

We study the optical modes in resonator structures obtained by assembling microcavities with a three-dimensional confinement of light. We used scanning confocal microscopy in order to measure light emission from these structures in the near optical field. Our studies give direct and detailed insight into the spatial distribution of the electromagnetic fields of confined modes in these photonic structures. We find similarities between the spatial modes of two coupled resonators and those of a diatomic molecule, and between modes of a chain of resonators and those of a periodic molecular crystal. In particular, we show that deviations of cavity size in the chain give rise to localized photonic modes which resemble impurity states in molecular crystals.

DOI: 10.1103/PhysRevB.66.115302

PACS number(s): 78.55.Cr, 42.50.Dv, 42.60.Da

**I. INTRODUCTION**

The three-dimensional confinement of light in resonator structures whose dimensions are comparable to the wavelength of light has attracted considerable interest during the last years, both for basic physics reasons as well as for potential novel applications. The recent development of such resonators has opened the pathway to cavity quantum electrodynamics studies in solid-state systems. For example, an enhancement and a suppression of the spontaneous emission from semiconductor quantum dots embedded in these microcavities have been demonstrated.<sup>1</sup> The formation of quasideterministic single-photon sources have been demonstrated that are based on single semiconductor quantum dots embedded within a circular resonator or a microdisk.<sup>2</sup> Further, highly efficient lasers have been fabricated by an asymmetric deformation of microdisk-based lasers.<sup>3-5</sup>

One of the approaches for achieving efficient three-dimensional confinement of light is the lateral patterning of planar microresonators. The spectrum of the emitted light from these resonators, termed micropillars or photonic dots, is dominated by sharp resonances. The energies of these resonances strongly depend on the resonator dimensions. These systems are particularly compatible with applications, since they emit light in vertical direction, a desirable feature for efficient coupling to fibers.

These resonators can be used, in turn, as building blocks of more complicated structures. For example, by coupling two photonic dots by a narrow channel, “photonic molecules” have been fabricated. Their optical-mode spectrum shows strong similarities to the bonding and antibonding orbitals in diatomic molecules.<sup>6</sup> Isomeric molecules can be obtained by assembling several resonators in different geometries.<sup>7</sup> Further, by coupling an increasing number of

resonators in a linear chain the transition from an atomlike system with a discrete mode spectrum to a crystal-like system with a band structure has been demonstrated.<sup>8</sup> Defects in these periodic crystals can be realized by varying the size of one of the resonators in the chains.<sup>9</sup>

There are two main ways to obtain insight into the electric-field distributions in these micrometer-sized structures: (i) The far-field emission intensity is given by the square of the Fourier transform of the field distribution in the resonator plane. Thus the field can be observed by detecting the emission far away from the resonator. (ii) The field distribution can be measured in the near field directly in experiments with high spatial resolution such as confocal microscopy or near-field scanning microscopy. We note here that near-field measurements refer to the characteristic dimensions of the resonators, and not directly to the optical wavelength.

Previously, we relied on the first technique only, and in conjunction with detailed numerical calculations we studied the field distributions in these photonic structures. In this work, we present the results of similar studies which are based on direct measurements of the spatial distribution of the electromagnetic field intensity using diffraction limited confocal microscopy. After describing the experimental setup in the next section we discuss data obtained for photonic molecules in the third section, while in the fourth section the field distributions for photonic chains without and with “defects” is presented and discussed.

**II. EXPERIMENT**

A conventional planar semiconductor cavity consisting of a GaAs  $\lambda$  resonator sandwiched between highly reflecting Bragg mirrors made from 21 (23) alternating GaAs and AlAs

quarter wave stacks was used for fabricating the confined photon geometries. A 7-nm-wide  $\text{In}_{0.14}\text{Ga}_{0.86}\text{As}$  quantum well which serves as the optically active medium was placed in the resonator at the antinode of the electric-field distribution. Photonic molecules and crystals were obtained from these planar cavities by electron-beam lithography and subsequent reactive ion etching. More details about these systems have been given elsewhere.<sup>6</sup>

For the near-field optical studies, the structures were mounted on a helium flow cold finger cryostat which was a part of a diffraction limited low-temperature confocal optical microscope. The microscope consists of a  $\times 60$  *in situ* microscope objective which focuses the tunable continuous wave (cw) Ti:sapphire laser light at normal incidence on the sample. The emitted light is then collected by the same microscope objective which can be accurately manipulated in three directions using computer controlled motors. The collected light is spatially filtered, dispersed by a 0.5-m monochromator and detected by a nitrogen cooled charged-coupled device (CCD) array detector. The system provides diffraction limited spatial resolution both in the excitation and the detection channels. We tested the combined spatial resolution of our system by creating selective photoluminescent (PL) images of the cleaved edge of a single quantum well sample.<sup>10</sup> The spatial full width at half maximum of the PL emission intensity was found to be 0.5–0.6  $\mu\text{m}$ , in agreement with the expected diffraction limited optical resolution at this wavelength ( $\approx 750$  nm). The collection efficiency of our system was carefully obtained from the measured spectrum of the reflected laser beam.

For the studies reported below we used high-energy non-resonant excitation ( $\approx 750$  nm). This excitation generates  $e$ - $h$  pairs within the GaAs/AlGaAs layers of the structure. The pairs diffuse into the  $\text{In}_{0.14}\text{Ga}_{0.86}\text{As}$  quantum well (QW), where they radiatively recombine and thereby build the electromagnetic radiation field of the entire photonic structure. The size of the excitation spot is therefore irrelevant to the studies reported below and the same results would have been obtained if the diffraction limited spatial resolution was applied to the collection channel only.

### III. PHOTONIC MOLECULES

The inset to Fig. 1 shows the side view of a photonic molecule structure as obtained by a scanning electron microscope. The size of each resonator is  $3 \times 3 \mu\text{m}$ . The interconnecting channel is 0.5  $\mu\text{m}$  long and 2  $\mu\text{m}$  wide. The spatially integrated emission spectrum from such a “photonic molecule” is shown in Fig. 1. The broad emission band centered at about 1.397 eV corresponds to the emission from the ground-state exciton in the  $\text{In}_{0.14}\text{Ga}_{0.86}\text{As}$  quantum well. At lower energy, several rather sharp spectral lines are observed. These lines are due to emission from three dimensionally confined modes of the electromagnetic radiation within the photonic molecule. We label each mode by a number for a later reference. The energy separation between the lowest energy mode and the excitonic emission exceeds 10 meV. Therefore these cavity polariton modes are weakly coupled to the ground exciton states. Thus in the following consider-

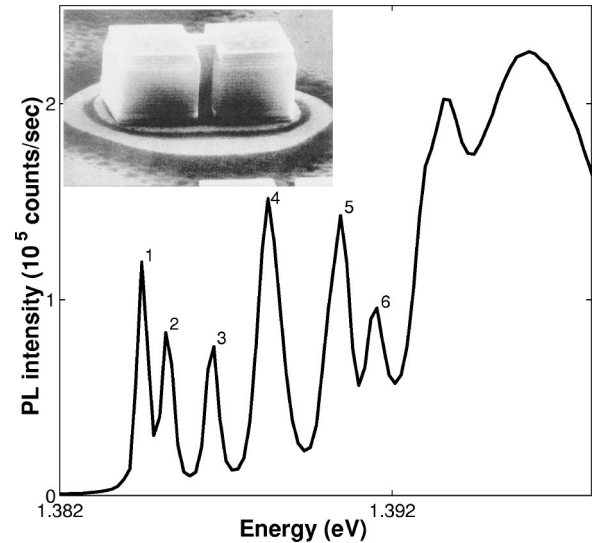


FIG. 1. Spatially integrated emission spectrum of the photonic molecule, the scanning electron micrograph of which is shown in the inset. The numbers indicate spectral lines due to PL from the discrete photonic modes of the structure.

ations of the field distributions weak coupling between the exciton and cavity modes is assumed.<sup>11</sup>

In Fig. 2(a) we present the image of the photonic molecule as obtained by our scanning confocal microscope using spectrally nonresolved reflected white light from the molecule surface. As expected [see the sketch of the silhouette of the molecule structure in Fig. 2(f)] for this mode of operation, which we use for calibrating purposes only, the intensity of the reflected light is almost homogeneously distributed over the structure’s surface. In Figs. 2(b)–(e) we present four selective wavelength confocal microscopy PL images of the photonic-molecule. The images are associated with the four lowest lying spectral modes (1–4) in Fig. 1(b). These gray-scale images are obtained from the PL emission integrated over the spectral linewidth at half the maximum of each mode spectral line as a function of the microscope objective position. Bright (dark) colors indicate regions of high (low) intensity, respectively, as shown by the gray-scale bars in the figure. For comparison the calculated spatial distribution of the electromagnetic field for these modes are displayed in Figs. 2(g)–(j), respectively. These calculations were made by solving Maxwell’s equations for the electromagnetic modes of these structures using the boundary element method.<sup>12</sup>

In Fig. 3 the measured near-field information is presented in a somewhat more insightful way. The PL intensity is presented as measured along the molecule symmetry axis as a function of the microscope objective position along this line and as a function of the detection energy. While the exciton emission shows a rather weak spatial dependence, the optical modes depend strongly on the position along the molecule axis. This dependence reflects the distribution of their electromagnetic fields. The various optical modes in each of the two resonators can be characterized by the notation  $(n_x, n_y)$ , where the  $n_i$  give the number of nodes in the electric-field distribution along the corresponding direction in the resona-

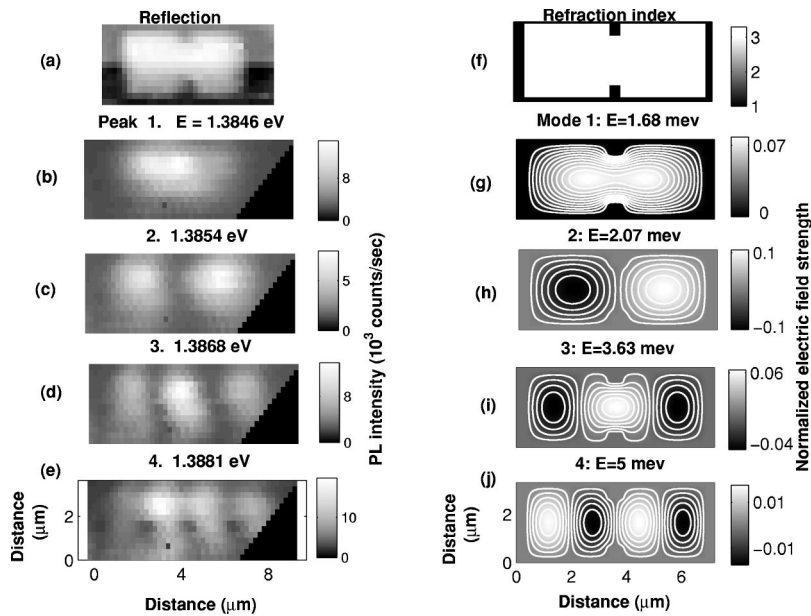


FIG. 2. (a) The photonic molecule shape as measured by the scanning confocal microscope using the reflection of its own white light. (b)–(e) Selective wavelength PL images of the photonic molecule. The PL intensity at each of the first lowest energy photonic modes is displayed using a grey color scale as a function of the microscope position above the structure. (g)–(j) Calculated eigenenergy and spatial distribution of the intensity of the electromagnetic field of the lowest energy modes of the structure. The calculated energies represent light “confinement” energies (Ref. 12). The geometrical shape of the photonic molecule, as should have ideally been seen by the reflected light, is shown in (f) by the spatial distribution of its refraction index.

tor plane. We assign here the  $x$  direction to the molecule axis.

The two lowest states correspond to the symmetric and antisymmetric modes that arise from the (0,0) mode in the separate resonators. The field distribution of these modes shows strong similarities to the bonding and antibonding  $\sigma$ -like molecular orbitals in diatomic molecules (like the hydrogen molecule) that originate from hybridization of the  $s$  orbitals of the atoms. The observed distributions of the emis-

sion intensity compare well with the ones from the calculated field distributions in Figs. 2(g)–(j).

The behavior becomes more complicated for the higher modes. Whereas mode 3 can be easily identified as the  $\sigma$ -like “bonding” orbital that originates from coupling of the (1,0) modes, for the next higher energy mode an identification is less clear. Its emission seems to be dominated by the “anti-bonding” orbitals of mode 3. There seem to be, however, also contributions from other modes that most probably are the symmetric and antisymmetric modes arising from coupling of the (0,1) or the (1,1) photonic dot modes. This qualitative description is supported by the width of the corresponding spectral line in Fig. 1(b), which is broader than that of modes 3 and 5, for example. Mode 5 in Fig. 3(b) shows five distinct maxima, which allows us to attribute it to the symmetric molecule mode connected with the (2,0) mode. Mode 6 shows already a significant contribution from the broad exciton emission which causes a large spectral linewidth and prevents a clear assignment to a particular optical mode in the coupled resonator structure.

#### IV. PHOTONIC CRYSTALS

We now turn to study linear chains of coupled resonators. It was previously demonstrated<sup>8</sup> that a chain of 12 coupled resonators resembles to a large degree an infinite one-dimensional (1D) photonic crystal structure. For example, it was shown that like in the case of an infinite structure, there are energy ranges (bands) in which light can propagate along the chain, and that in between these ranges there are gaps (band gaps), in which light cannot propagate. Increasing the chain length by adding more resonators did not result in a noticeable change to the bandlike energy structure of these photonic crystals.<sup>8</sup>

##### A. Crystals without defects

Figure 4(a) shows a scanning electron micrograph of such a chain consisting of photonic dots with lateral dimensions of

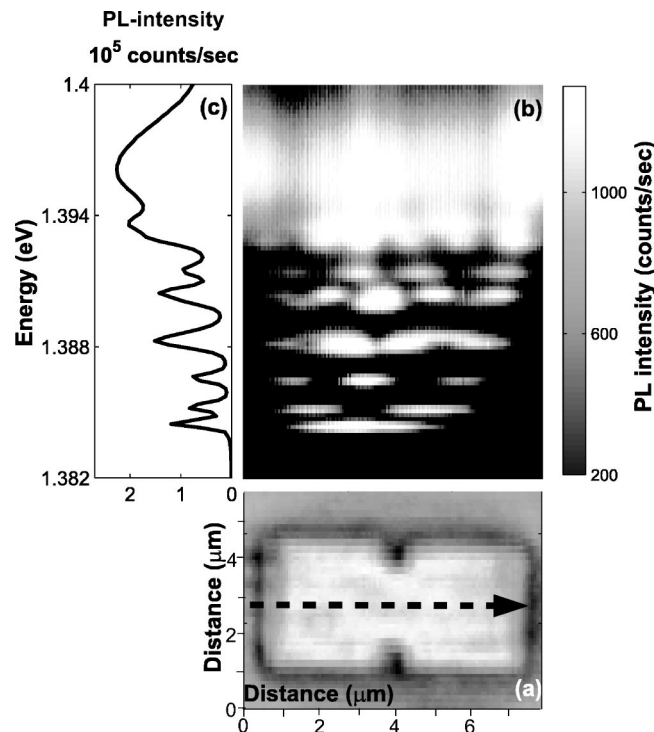


FIG. 3. (a) An optical microscope picture of the photonic molecule. (b) The PL spectra as a function of the microscope position along the symmetry axis of the photonic molecule as shown in (a). (c) The spatially integrated spectrum of the molecule.

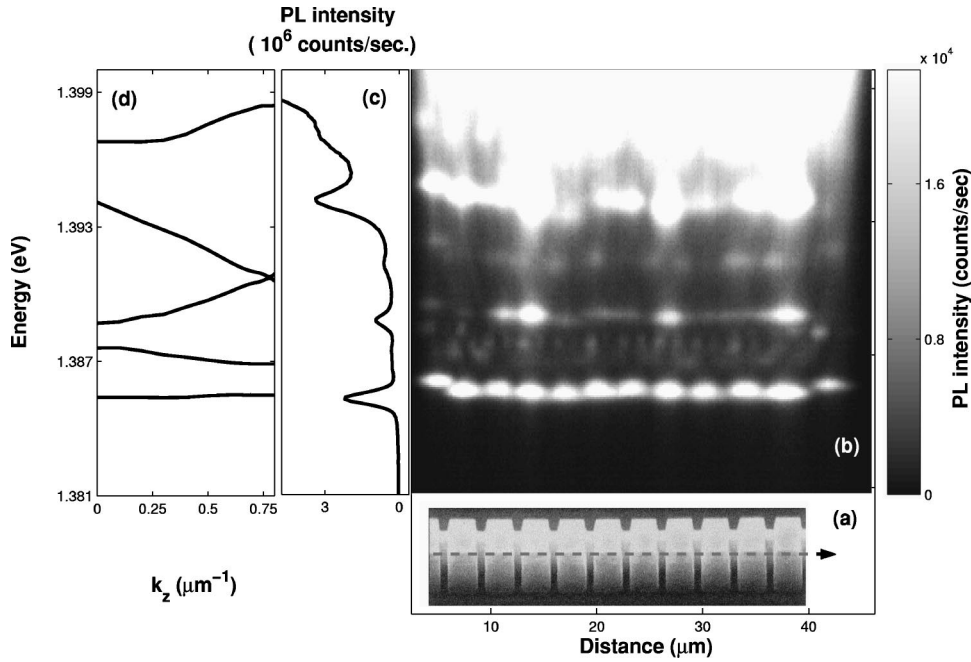


FIG. 4. (a) Scanning electron micrograph of a photonic chain (the resonators at the edges are not seen). (b) The PL spectra as a function of the microscope position along the symmetry axis of the photonic chain as shown in (a). (c) The spatially integrated PL spectrum of the chain. (d) The calculated energy dispersion vs the chain crystal momentum along its axis, presented in its first Brillouin zone (Ref. 11).

$3 \times 3 \mu\text{m}$ . The interconnecting channels are  $1 \mu\text{m}$  long and  $1.5 \mu\text{m}$  wide. In Fig. 4(b) we present the results of a confocal microscopy PL line scan along such a chain. The spatially integrated PL spectrum is displayed in Fig. 4(c), and the calculated mode energies vs the chain “crystal momentum” along its axis, within the first Brillouin zone are presented for comparison in Fig. 4(d). Five main different energy modes below the energy of the exciton are observed in Fig. 4(b). The electromagnetic field distributions, associated with these modes extend over the whole chain. We believe that the intensity of the emission from these modes is determined by the interplay of (i) polaritons thermalization towards the ground modes (which depends on the coupling to the exciton mode), (ii) the energy separation from the exciton, which determine the coupling strength and possible thermalization channels, (iii) the energy and density of the band modes in the zone center, and (iv) local variations and imperfections in the chain properties. In contrast to photonic dots, the thermalization of photogenerated carriers in the chain maybe quite efficient due to the quasicontinuous nature of its mode spectrum, which is different from the discrete nature of photonic dots.

The five observed spectral features are separated by gaps of  $\sim 2.1$ ,  $\sim 1.7$ ,  $\sim 2.6$ , and  $\sim 2.7$  meV, respectively. To understand their origin, we display in Fig. 4(d) the calculated dispersion of the chain modes as a function of the mode spatial phase between the coupled resonators (the equivalent of crystal momentum in crystals). In the optical far field, this energy dispersion was directly measured using angle-resolved spectroscopy.<sup>11</sup> In this study, the objective of the confocal microscope collects emission in the near field (near means closer than the dimensions of the resonators) from modes which cover a range of wave numbers in close vicinity to  $k_z=0$  only. As shown in Fig. 4(d), in this region of  $k$ , the chain bands are rather flat and therefore their density of modes peaks. Thus our study maps the spatial distribution of

the zone-center modes mainly. This is evident from the energy width of the five modes in Figs. 4(b) and (c). The linewidths are almost the same, in spite of the considerable difference in the various bands dispersion.<sup>11</sup>

The lowest mode, at energy of 1.3854 meV, has emission maxima in each of the resonators and minima in the channels between them. We associate this mode with the Brillouin-zone center edge of the lowest band in the corresponding infinite chain, as shown in Fig. 4(d). From our calculations it follows that the zone-center second band edge of the infinite chain lies  $\sim 2.3$  meV above this energy, in excellent agreement with our observation of a very weakly emitting mode at this energy. As expected, this mode has two maxima and one minima in each resonator. We note that the second and fourth bands are considerably weaker than the first, third, and fifth bands. The reason for this phenomenon can be understood by inspecting Fig. 4(d). The zone-center modes of the even bands are the highest energy modes within these bands, while the zone-center modes of odd bands are the lowest energy ones. Thermalization of polaritons within the bands may thus play an important role in weakening the near-field emission from the even bands and strengthening the emission from the odd bands. In addition, the even bands are less flat in the zone center, and therefore the density of their modes there is lower than that of the odd bands.

The higher energy spectral features originate from the zone-center edges of the third, fourth, and fifth bands, respectively. While the energy of the third band agrees quite well with our calculations, these of the fourth and fifth band do not. The discrepancy may be attributed to the fact that the coupling of the electromagnetic modes to the exciton is neglected in our calculations. This coupling is more important for the higher energy modes, which are closer to the exciton energy.<sup>8</sup> The detailed spatial intensity distribution of these higher energy modes on a scale of one resonator is not very well resolved in the line scan of Fig. 4(b). We believe that

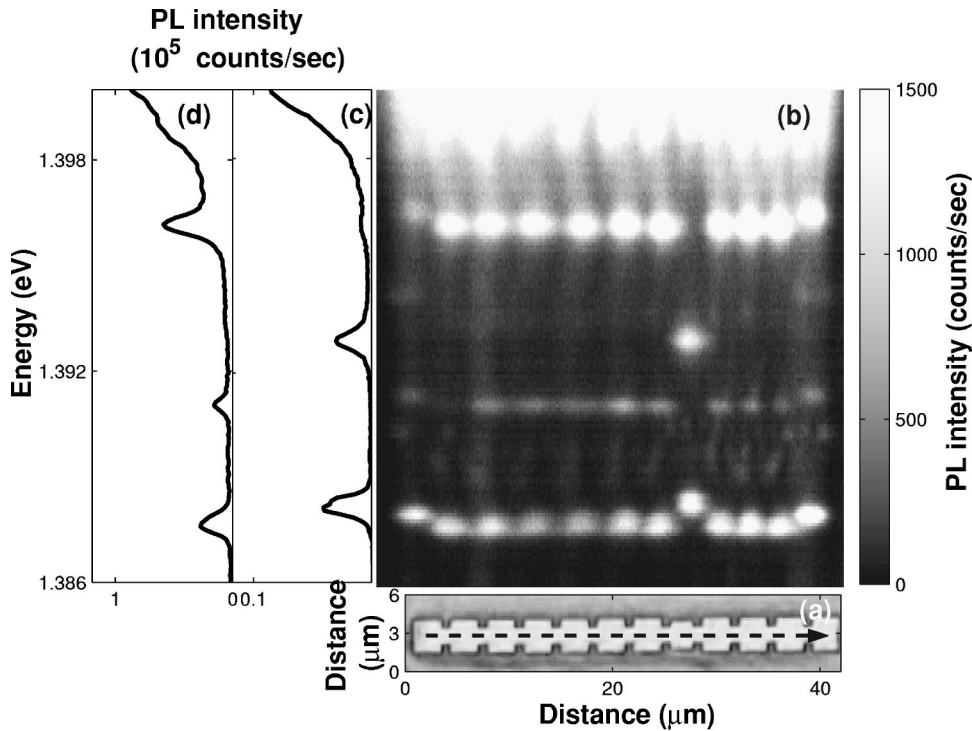


FIG. 5. (a) Optical microscope micrograph of a photonic chain with a smaller resonator (b) The PL spectra as a function of the microscope position along the symmetry axis of the photonic chain as shown in (a). (c) Respectively; (d) spatially integrated spectrum from the smaller resonator respectively four resonators left to it.

this is mainly due to lack of resolution, and increased dispersion within the bands. We note here that the observation of band structure in general and the clear distinction between odd and even bands in particular demonstrates that we probe collective emission modes of all the resonators within the chain. This is in spite of the local nature of our confocal microscope excitation.

Most remarkably, the emission from the two resonators at each end of the chain is slightly shifted towards higher energies, as seen both for the lowest and for higher energy bands. Obviously, this is due to the finite length of the 1D photonic crystal. The edge resonators do not possess translational invariance of an ideal crystal. In this sense, the two edge resonators deviate the most from the rest of the resonators, and they can be considered as defects or “surface states” in the crystal. Intuitively this phenomenon can be explained in the following way: Whereas the field distribution in a regular chain element penetrates considerably into its neighboring elements, it is sharply terminated by the chain edge in the outer resonators. Consequently the mode volume is slightly smaller for these resonators, resulting in a shift of 0.6 meV of the mode towards higher energy. Another useful description of these surface-state-like defects is in terms of acceptor like states with an energy slightly above the edge of the rather flat valence band of the photonic crystal. The calculated electric-field distribution of these edge modes (not shown) resemble the measured ones in their spatial shape. The calculated energy of the lowest energy edge mode, however, is only 0.1 meV above the “valence” band of the photonic crystal and the corresponding mode has maximum intensity in the edge resonators, yet they penetrate quite significantly into adjacent chain elements.

### B. Crystals with defects

In order to study the field distribution when a defect is incorporated into the periodic crystal we measured two

modified photonic chains, one with a smaller resonator and one with a larger one. The first chain is shown in Fig. 5(a), where the width of the fifth resonator in the chain is reduced to  $2.5 \mu\text{m}$ . The sizes of all the other parameters were the same as in the chain without defects. In Ref. 9 it was shown that this size reduction leads to an acceptorlike state in the first band gap. The localization of this mode is clearly evidenced in the confocal microscopy PL line scan shown in Fig. 5(b). The emission energy of this mode ( $E = 1.3883 \text{ eV}$ ) is slightly above the energy of the top photonic crystal valence band ( $E = 1.3881 \text{ eV}$ ). The mode is strongly localized around the defected resonator and its penetration into the neighboring chain elements is rather weak. The mode energy and distribution agree well with the calculated energy (0.6 meV) and electric-field distribution (not shown). A higher energy, localized defect mode is also observed at 1.3932 eV, in the gap between the conduction bands of the corresponding infinite system. This high-energy localized mode was not observed in previous far-field measurements.<sup>9</sup>

In Figs. 5(c) and (d) we compare the spatially integrated spectrum measured at the smaller resonator [Fig. 5(d) with that in the photonic crystal to its left side [Fig. 5(c)]. We note that at the smaller resonator the emission from the crystal modes is strongly suppressed. Consequently, almost the whole emission from the defect comes from its localized modes.

Figure 6(a) describes a photonic chain structure, in which the dimensions of the fifth resonator have been enlarged to  $5.5 \times 5.5 \mu\text{m}$  as compared to the regular chain elements of  $3 \times 3 \mu\text{m}$ . As a consequence of this enlargement, a large number of localized modes appear in the spectrum, as can be seen in the PL line scan along the crystal center in Fig. 6(b). There are two modes below the first (valence) band, which

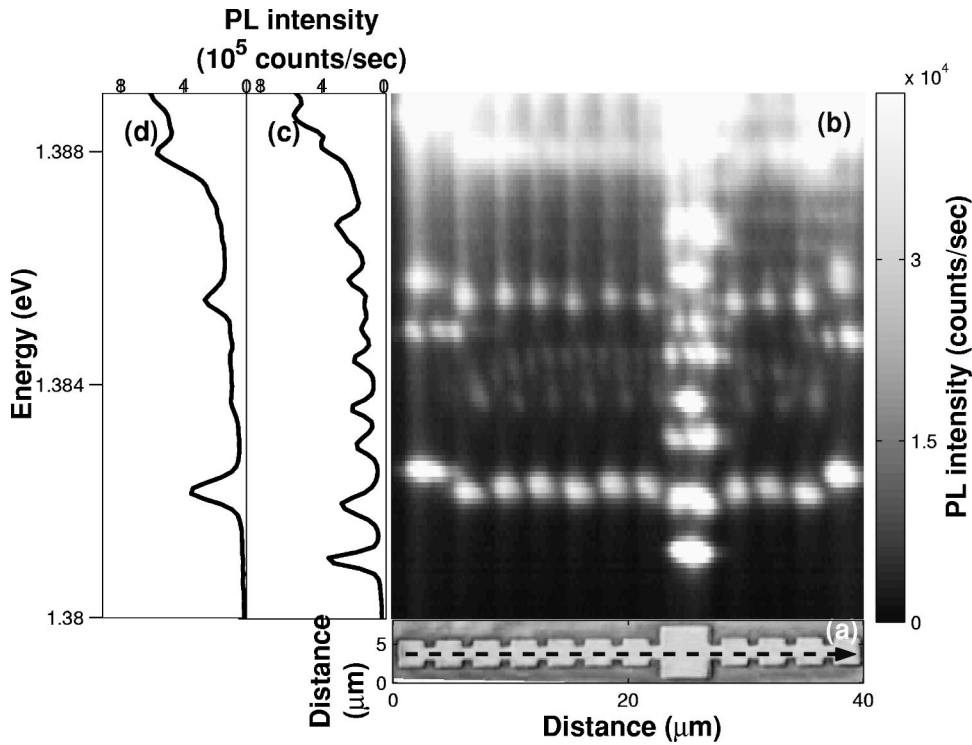


FIG. 6. (a) Optical microscope micrograph of a photonic chain with a larger resonator. (b) The PL spectra as a function of the microscope position along the symmetry axis of the photonic chain as shown in (a). (c) respectively (d) spatially integrated spectrum from the larger resonator respectively four resonators to its left side.

are concentrated in the enlarged resonator. Four such modes are observed between the first and the third band edges and few similar higher energy modes above the second chain band. More information about the field distributions of the various modes in the vicinity of the defect can be readily obtained from the selective wavelength images of the defects depicted in Fig. 7. The six bottom panels in Fig. 7 show enlargements of the field distributions of six different defect modes. The modes are labeled by numbers in increasing emission energy order as shown in the spatially integrated spectrum in the top panel of Fig. 7. The lowest mode (peak 1), at energy of 1.3807 meV, has a symmetric distribution slightly elongated along the chain axis. It does not have nodes, and thus it resembles the (0,0) mode of an isolated photonic dot. The second mode, 0.8 meV above the first mode, has a nodal plane perpendicular to the chain axis. One may associate it with a (1,0) mode of an isolated resonator. The third mode, 1.2 meV above the lowest mode, has a nodal plane parallel to the chain axis. Therefore it can be associated with a (0,1) mode of an isolated resonator. The field distribution of the fourth mode, 2.1 meV above the first one, has two perpendicular nodal planes. Therefore it resembles the (1,1) mode of an isolated resonator. The fifth mode in energy order, 2.9 meV above the first mode, has two nodal planes parallel to the chain axis and no nodes parallel to it. Similarly, it can be associated with a (0,2) mode of an isolated resonator. The sixth mode has energy of 4.1 meV above the lowest energy mode. The mode seems to have one nodal plane perpendicular to the chain axis and a more complicated structure in planes which are parallel to the chain. This, and other higher energy modes (not shown), are more complicated structurally, possibly due to stronger coupling to the extended chain modes. We made no attempt to describe these modes in terms of the intuitive and simple modes of an iso-

lated resonator. We note, that modes 2 and 6 can be hardly observed in the spatially integrated spectrum [Fig. 7(a)]. This behavior indicates mode leakage into neighboring resonators. As indeed expected for modes with similar symmetry to the modes of the chain's valence band.

For comparison with the measurements, the calculated electric-field distributions and energies of the first six lowest energy defect modes are shown in Fig. 8. The calculated, lowest energy mode has a symmetric field distribution without any nodes, thus it resembles the (0,0) mode of an isolated photonic dot. The mode is mostly concentrated in the defect, and only weakly penetrates into neighboring resonators. It is more circular than the measured one, which is rather elongated. Similarly, the next three higher energy modes can be described in these terms as the isolated resonator ("impurity") (1,0), (0,1), and (1,1) modes at energies of 0.91, 1.03, and 1.98 meV above the ground (0,0) mode, respectively. These calculated energies and distributions agree quite well with the experimental observations of Fig. 7. In particular we note that the second mode significantly penetrates into neighboring resonators, in agreement with its absence in the spatially integrated spectrum [Fig. 7(a)]. The fifth calculated mode, at energy of 2.91 meV deviates from the fifth measured one. The latter resembles both in its energy and spatial distribution the calculated sixth mode. We believe that this discrepancy has to do with our spectral resolution (0.15 meV) which prevents us from spatially distinguishing between energy modes close to the 1D continuum of the photonic crystal.

## V. SUMMARY

We used low-temperature, scanning confocal microscopy to map the spatial distribution of the electromagnetic fields in

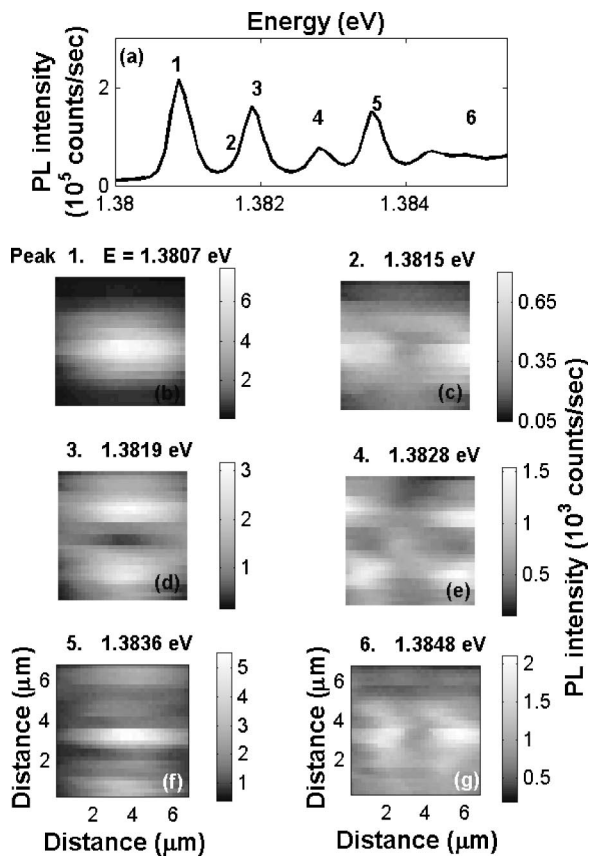


FIG. 7. (a) Spatially integrated emission spectrum from the larger resonator in a photonic chain of resonators. The numbers indicate spectral lines due to PL from the discrete photonic modes of the “defected” resonator. (b)–(g) Selective wavelength PL images of the resonator in a photonic chain of resonators. The PL intensity at each of the six lowest energy photonic modes is displayed using a grey color scale as a function of the microscope position above the resonator.

various photonic structures. The structures were assembled from semiconductor microcavity resonators which were laterally patterned by electron-beam lithography in order to achieve light confinement in three dimensions.

We demonstrated that our technique can directly measure the spatial distributions of the electromagnetic fields of discrete confined optical modes in these photonic structures.

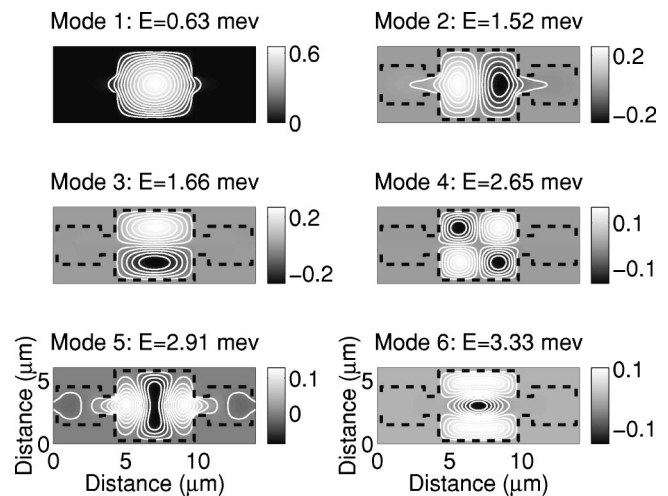


FIG. 8. Calculated mode confinement energy and contour plots of the electric-field distributions of the six lowest energy modes around a  $5.5\text{-}\mu\text{m}$ -square cavity embedded in a chain consisting of 12 coupled square photonic dots of  $3\ \mu\text{m}$  (Ref. 12). The resonators are connected by a channel with  $1.0\ \mu\text{m}$  length and  $1.5\ \mu\text{m}$  width. The dotted lines indicate the boundaries of the chain structure.

The measured electromagnetic field maps were found to be in good agreement with numerical calculations for solutions to Maxwell’s equations. We note that the picture obtained here by directly measuring the spatial distribution of the electromagnetic radiation field is more detailed than the one obtained indirectly, using far-field, angle-resolved spectroscopy.<sup>6,9</sup>

We presented striking similarities between the distributions of the electromagnetic fields in these photonic structures and the wave functions of electrons in molecular structures. In particular, it was demonstrated that irregularities in the periodic structure of a one-dimensional chain of coupled resonators give rise to localized photonic modes which resemble localization by impurities in molecular crystals.

## ACKNOWLEDGMENTS

This work was supported by the German-Israeli Foundation, by the Deutsche Forschungsgemeinschaft, by the State of Bavaria, by the U.S. Office of Naval Research, and by DARPA.

\*Present address: Experimentelle Physik II, Universitaet Dortmund, D-44221 Dortmund, Germany.

<sup>1</sup>For the enhancement of the spontaneous emission, see J.M. Gérard, B. Sermage, B. Gayral, B. Legrand, E. Costard, and V. Thierry-Mieg, *Phys. Rev. Lett.* **81**, 1110 (1998); for the suppression, see M. Bayer, T.L. Reinecke, F. Weidner, A. Larionov, A. McDonald, and A. Forchel, *ibid.* **86**, 3168 (2001).

<sup>2</sup>J. Kim, O. Benson, H. Kan, and Y. Yamamoto, *Nature (London)* **397**, 500 (1999); P. Michler, A. Kiraz, C. Becher, W.V. Schoenfeld, P.M. Petroff, L. Zhang, E. Hu, and A. Imamoglu, *Science* **290**, 2282 (2000); C. Santori, M. Pelton, G. Solomon, Y. Dale, and Y. Yamamoto, *Phys. Rev. Lett.* **86**, 1502 (2001); E. Moreau,

I. Robert, J.M. Gérard, I. Abram, L. Manin, and V. Thierry-Mieg, *Appl. Phys. Lett.* **79**, 2865 (2001).

<sup>3</sup>C. Gmachl, F. Capasso, E.E. Narimanov, J.U. Nöckel, A.D. Stone, J. Faist, D.L. Sivco, and A.Y. Cho, *Science* **280**, 1556 (1998).

<sup>4</sup>J.M. Gérard, D. Barrier, J.Y. Marzin, R. Kuszelewicz, L. Manin, E. Costard, V. Thierry-Mieg, and T. Rivera, *Appl. Phys. Lett.* **69**, 449 (1996).

<sup>5</sup>J.P. Reithmaier, M. Rhner, H. Zull, F. Schfer, A. Forchel, P.A. Knipp, and T.L. Reinecke, *Phys. Rev. Lett.* **78**, 378 (1998).

<sup>6</sup>M. Bayer, T. Gutbrod, J.P. Reithmaier, A. Forchel, T.L. Reinecke and P.A. Knipp, *Phys. Rev. Lett.* **81**, 2582 (1998).

<sup>7</sup>G. Guttroff, M. Bayer, A. Forchel, P.A. Knipp and T.L. Reinecke,

- Phys. Rev. E **63**, 036611 (2001).
- <sup>8</sup>M. Bayer, T. Gutbrod, A. Forchel, T.L. Reinecke, P.A. Knipp, R. Werner, and J.P. Reithmaier, Phys. Rev. Lett. **83**, 5374 (1999).
- <sup>9</sup>G. Guttroff, M. Bayer, J.P. Reithmaier, A. Forchel, P.A. Knipp, and T.L. Reinecke, Phys. Rev. B **64**, 155313 (2001).
- <sup>10</sup>T.D. Harris, D. Gershoni, R.D. Grober, L.N. Pfeiffer, K.W. West, and N. Chand, Appl. Phys. Lett. **68**, 988 (1996).
- <sup>11</sup>T. Gutbrod, M. Bayer, A. Forchel, J.P. Reithmaier, T.L. Reinecke, S. Rudin and P.A. Knipp, Phys. Rev. B **57**, 9950 (1998); **59**, 2223 (1999).
- <sup>12</sup>P.A. Knipp and T.L. Reinecke, Phys. Rev. B **54**, 1880 (1996); Physica E (Amsterdam) **2**, 920 (1998).